
Article:
Langdon, G.S. orcid.org/0000-0002-0396-9787, Gabriel, S., von Klemperer, C.J. et al. (1 more author) (2021) Transient response and failure of medium density fibreboard panels subjected to air-blast loading. Composite Structures, 273. 114253. ISSN 0263-8223

https://doi.org/10.1016/j.compstruct.2021.114253

Transient response and failure of medium density fibreboard panels subjected to air-blast loading

G.S. Langdon[1,2], S. Gabriel[2], C.J. von Klemperer[3], S. Chung Kim Yuen[2]

[1]*Department of Civil and Structural Engineering, University of Sheffield, Sheffield, S1 3JD, UK*

[2]*Blast and Impact Survivability Research Unit (BISRU), Department of Mechanical Engineering, University of Cape Town, Rondebosch, 7700, South Africa.*

[3]*Department of Mechanical Engineering, University of Cape Town, Rondebosch, 7700, South Africa.*

Abstract

This paper presents insights into the response and failure of medium density fibreboard (MDF) panels subjected to air-blast loading. The MDF panels are representative of a cheap, and potentially sustainable, structural material that is commonly used in homes and buildings. Simplified computational simulations were used to design a series of air-blast experiments to elucidate a range of responses and failures within the MDF. The blast-loaded MDF panels exhibited multiple surface cracks, substantial in-plane cracking throughout the less dense parts of the cross-section, and fragmentation failures. The transient results show MDF exhibits peak displacement that are many times greater than the permanent deformation, and that the internal damage due to cracking reduced the stiffness of the panels. These findings provide unique and detailed insights into the cracking and fragmentation of MDF that will prove valuable to blast protection engineers considering the effects of explosive detonations inside buildings containing MDF furnishings, and any increased risk of secondary blast injuries due to flying MDF debris. The experimental data can be used by modellers to validate simulations of damage due to explosive events in the future.

Keywords: wood fibre based composites, medium density fibreboard; blast response; fragmentation; cracking failure.

1. Introduction

Terrorism remains a significant and serious threat in the eyes of the public across the world [1], with bombings in Sri Lanka (2019) and Manchester (2017), among others, keeping the public aware of this devastating tactic. The Easter bombings in Sri Lanka occurred indoors, targeting churches, hotels and a housing complex [2]. Additionally, over 130 000 people were injured or lost their lives [3] during incidents involving improvised explosive devices over a five year period (2011-2016). Furthermore, the global economic impact of terrorism is high, estimated to be a staggering $26.4 billion in 2019 alone [1]. Sadly, accidental explosions also pose a risk, as demonstrated by recent disasters in China [4] and Beirut [5]. For example, the 2020 Beirut explosion had an explosive yield estimated to be 500-1120 T TNT equivalent [6]. More than 6000 people were injured and 181 people died. Social media footage filmed the blast propagating through the streets, demolishing buildings and destroying local homes and businesses.

The use of low cost alternative materials in the construction of furniture has led to the increasing popularity of engineered wood products like medium density fibreboard (MDF) and plywood [7-8]. MDF is one of the most widely used wood composites [7] as it offers dimensional stability (unless exposed to water), has consistent strength and stiffness properties, and is easy to paint or glue [7-11]. This makes it ideal for shelving, furniture, partition walls and laminated flooring [7-11]. Efforts are underway to improve the environmental profile of MDF [9], such as developing alternatives to the urea-formaldehyde resin used [10-11], adapting its processing to utilise plant waste materials [12], and MDF waste recycling [13]. There is also work into enhancing its strength and toughness for use as an alternative building material [14]. In summary, MDF is a common construction material found in homes and businesses, and is likely to remain so as it becomes more sustainable. Despite its ubiquity, little is known about its blast performance as most studies (for example, see references [7, 11-17]) examine quasi-static properties such as modulus of rupture, water absorption, and internal bond strength, and some limited impact testing [7]. Blast studies on wood-based materials are limited to timber structures and natural woods such as oak, birch, pine and aspen [18-20], field tests on full-scale steel framed E-glass coated wooden wall panels [21], and a numerical study on cross-laminated timber [22].

This paper reports the results of a primarily experimental study on the transient response and failure of commercially available MDF panels subjected to air-blast loading. Firstly, the properties of MDF are characterised at quasi-static rates of strain and a computational model is used to estimate an appropriate explosive charge mass range. Next, the results of nine air-blast experiments are reported: transient displacement response, surface damage and internal cross-section failure. Stereomicroscopy and SEM are used to elucidate additional information about the failures observed. The findings are relevant to those modelling material damage or injury risk due to explosive events in settings where MDF is commonly used, such as housing complexes and shopping centres.

2. Material properties

2.1 Composition

MDF typically comprises 80% wood fibre, 10% urea-formaldehyde resin, 10% water and 1% wax [14]. Wood chips are processed into fibres that are formed into boards using a dry hot-pressing technique. The multi-stage pressing cycle results in panel boards with zones of increased density on the outer faces and a core region of lower density and mechanical strength. For this work, an MDF known as “Supawood” was used as it was locally produced (in South Africa), cheap and readily available [23]. The material safety data sheet [24] states that the nominal composition of Supawood MDF is 82-84% wood, 8-10% UF resin, 5-8% water and a small quantity of paraffin wax, with nominal density in the range 560-830 kg/m^3.

Several sheets of 16 mm thick MDF board were purchased for material characterisation and blast loading experiments. The panels had an areal density of 12.5 kg/m^2, equivalent to a 1.6 mm thick steel sheet or a nominally 5 mm thick, 400 g/m^2 glass-fibre epoxy panel. The cross-section indicated outer regions of more densified fibres, shown in Figure 1a, that are consistent with a typical MDF manufacturing process. Small (10

mm x 10 mm) pieces were removed from the panel cross-section and viewed using scanning electron microscopy (SEM) with some typical images shown in Figure 1b and Figure 1c. The images showed densely packed, randomly oriented fibres, with little resin, which is typically expected for MDF. Some of the fibres look less well defined at higher magnification, Figure 1c, due to the specimen polishing process used in preparing samples for SEM.

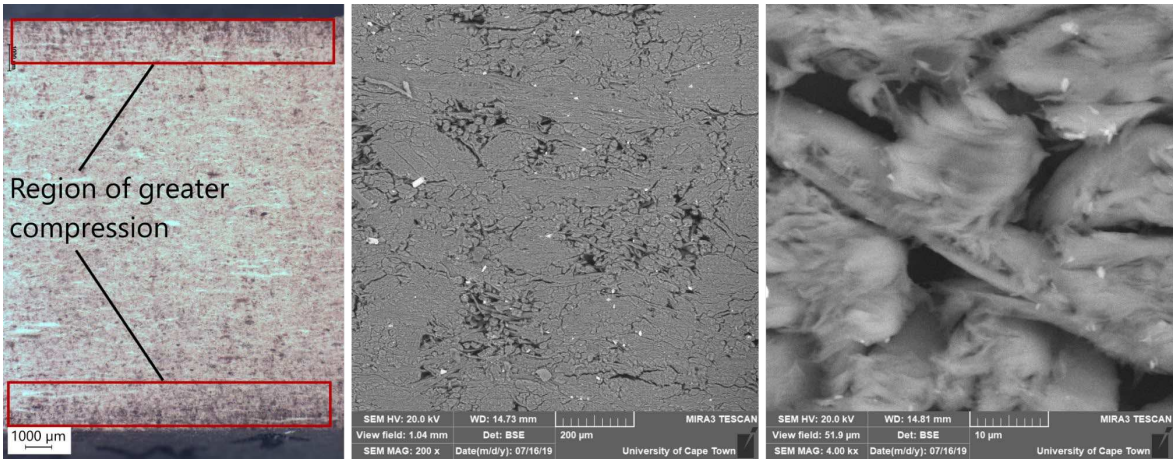

(a) (b) (c)

Figure 1: Photographs of a 16 mm thick Supawood MDF cross-section (a) taken using stereomicroscopy (b) SEM image at 200x (c) SEM image at 4000x

2.2 Flexural properties

Quasi-static 3-point flexural tests were performed on 55 mm wide, 260 mm long rectangular strips of Supawood MDF at a constant cross-head speed of 3 mm/min, in accordance with ASTM 7264 [25]. The engineering stress-strain relationship was curvilinear (Figure 2), with a mean average peak stress of 30±0.4 MPa at a strain of 0.015±0.0004 m/m. A steep drop in stress occurred after the peak, and failure occurred thereafter at an average strain of 0.017±0.001 m/m. The flexural modulus of elasticity was 27.6±0.03 GPa. The MDF specimens exhibited consistent flexural behaviour, evidenced by the low standard deviations.

2.3 In-plane tensile properties

The general tensile test procedure was based on ASTM D3039 [26], with specimens of 25 mm nominal width and 250 mm nominal length. The recommended specimen thickness of 2.5 mm was disregarded for the tests due to the changing density of the MDF throughout its cross-section. Specimens were cut at 0°, 45° and 90° to the length of the MDF board. Three types of specimen were tested: (1) 12 mm thick MDF from the core, with the outer surfaces shaved away, (2) 12 mm thick standard MDF board and (3) 3 mm thick MDF board. At least five specimens per configuration were tested. The face of the tensile specimen was coated with a speckle pattern

for filming. Digital image correlation was used to record the surface strain during the test. The crosshead speed was kept constant at 1 mm/min. To facilitate mounting in the grips and prevent slippage, the ends of the specimens were wrapped with emery cloth.

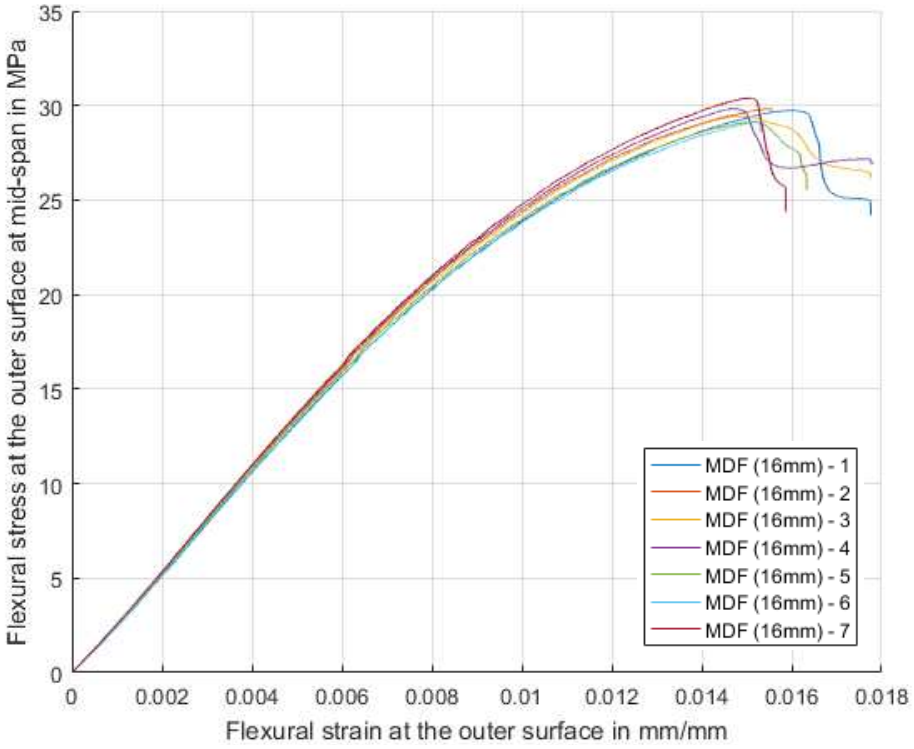

Figure 2: Typical engineering stress-strain curve obtained from quasi-static three point flexure tests on 16 mm thick Supawood MDF specimens

Lateral cracking was observed in all specimens, regardless of orientation, thickness or whether the outer surface was left intact or shaved away. In the 3 mm thick specimens, angled cracks were also observed for 0°, 45° and 90° specimens. The failure location varied, with some failures within the grip or within one width of it (this type of failure was more evident in "shaved" specimens and 45° specimens). When the results from specimens that failed close to the grip were discounted, the averages changed by up to 5%, within the variability of the properties. Overall, the MDF specimens exhibited brittle cracking failures and the engineering stress strain curves were curvilinear (Figure 3). The specimens with the outer surfaces present were strongest, with an ultimate tensile strength of 16.8 MPa, due to the denser fibres. As expected, the 12 mm thick specimens from the core (with the outer 2mm shaved away from each face of a 16 mm panel) were the weakest, with an average ultimate tensile strength of 7.8 MPa and a failure strain of 0.009 m/m. It appeared that most of the tensile strength of the MDF board was due to the outer 2 mm regions of the cross-section that comprise the denser fibre distribution. Similar trends were observed for modulus of elasticity as shown in the results summary in Table 1.

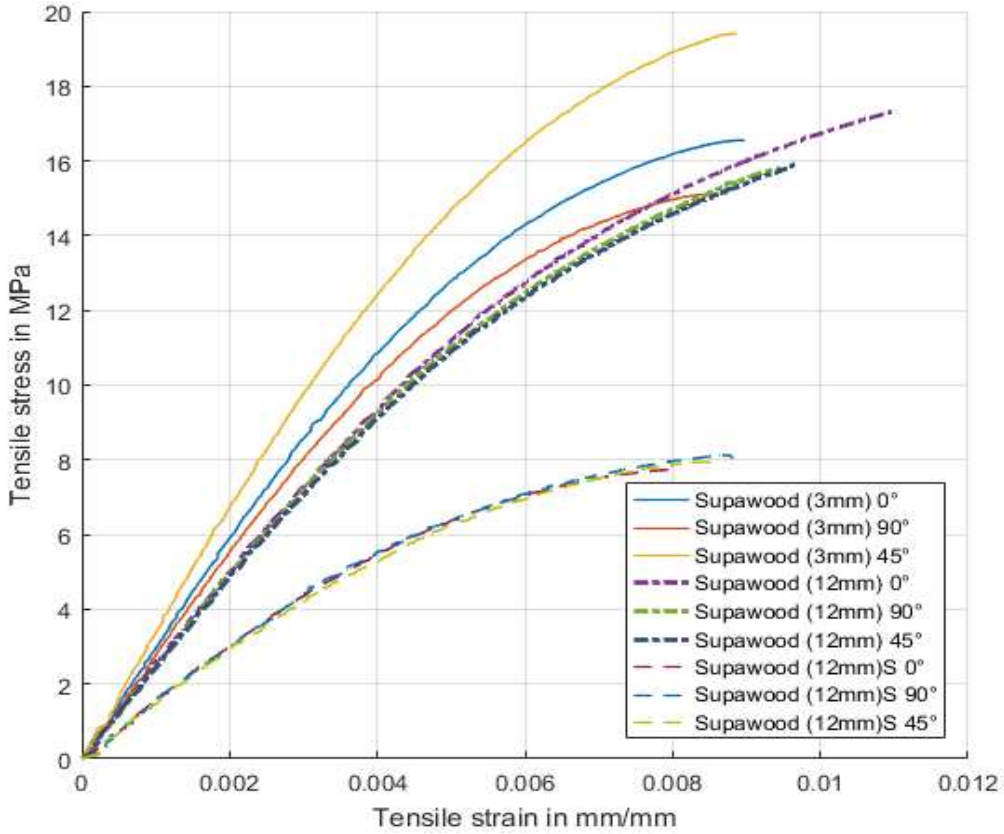

Figure 3: Engineering stress-strain curves obtained from in-plane tensile tests on Supawood MDF boards

Table 1: Summary of in-plane tensile test results

	Modulus of elasticity, E^T [GPa]		Apparent elastic limit, σ^T_Y [GPa]		Ultimate tensile strength, σ^T_U [MPa]		Strain at failure, ε^T_{fail} [m/m x10^3]	
	mean	*Std Dev*	*mean*	*Std Dev*	*mean*	*Std Dev*	*mean*	*Std Dev*
Supawood 3mm 0°	2.95	0.05	7.3	0.4	16.8	0.5	8.9	1.0
Supawood 3mm 90°	2.78	0.07	6.7	0.2	15.0	0.4	8.4	0.5
Supawood 3mm 45°	3.33	0.06	8.3	0.4	19.7	0.7	9.3	1.0
Supawood 12mm 0°	2.52	0.04	7.3	0.6	18.0	0.5	12.0	0.7
Supawood 12mm 90°	2.41	0.08	7.5	1.4	15.6	0.6	10.0	1.0
Supawood 12mm 45°	2.44	0.04	8.0	0.5	17.2	0.8	11.2	1.3
Supawood 12mm-S 0°	1.55	0.04	3.9	0.2	7.4	0.2	7.0	1.0
Supawood 12mm-S 90°	1.58	0.09	4.1	0.6	8.2	0.2	8.7	0.5
Supawood 12mm-S 45°	1.51	0.05	3.9	0.7	7.8	0.2	8.1	0.8

2.4 Through-thickness tensile properties

The through-thickness tensile tests were based on the SANS 6016 [27] standard. MDF blocks of 40 mm x 40 mm x 16 mm were glued into T-shaped steel loading blocks using a high-strength Spabond epoxy adhesive, shown in Figure 4. The assembly was mounted in a universal testing machine and the crossheads moved apart at a constant rate of 1 mm/min.

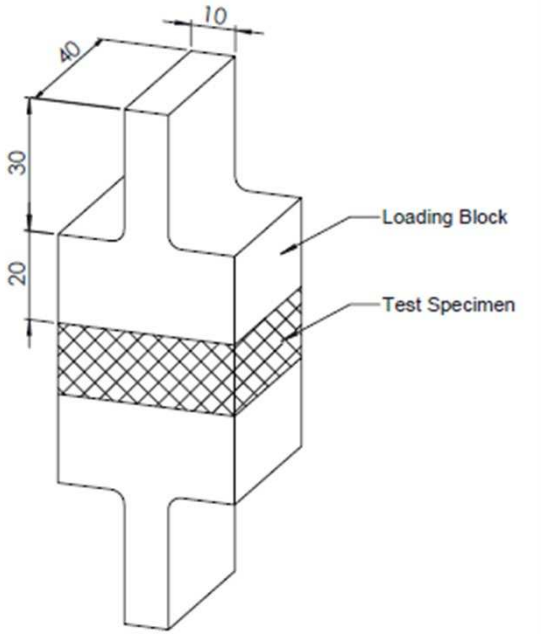

Figure 4: Schematic showing through-thickness tensile testing assembly

The mean average through thickness tensile strength was 0.38 MPa, based on five tests. The strengths varied considerably from 0.19 MPa to 0.69 MPa, possibly due to off-axis loading and mounting difficulties (although this may also reflect the natural variability of the material, this is unknown), so the manufacturer's nominal value of 0.5 MPa [24] seemed reasonable. Interestingly, the majority of specimens failed due to cracking near the mid-plane, shown in Figure 5, as expected since the core was less dense than the outer surfaces. .

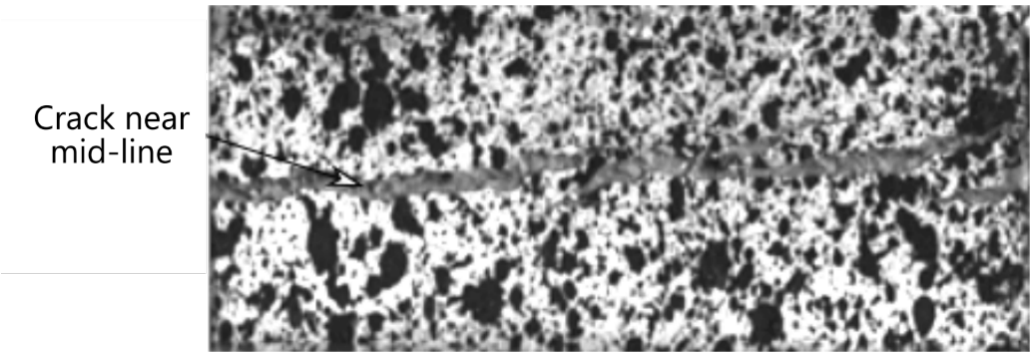

Figure 5: Photograph showing cracking failure of a through-thickness tensile test specimen

2.5 Through-thickness compression properties

Guidance for through-thickness compression testing was not present in the South African National Standard for uncoated fibreboard products [28] or ASTM standards [29] for evaluating properties of wood-based fibre and particle panel materials. Therefore, the square geometry recommended in reference [27] was adopted, with a side length of 25 mm that was large enough for many unit cells of MDF. A constant crosshead speed of 1 mm/min was used. Seven specimens were tested, with almost identical compressive properties obtained, shown in Figure 6. Response was approximately linear up to a strain of 0.007 m/m, followed by a steep increase in stress up to failure at a strain of 0.0171±0.0001 m/m. The mean average through-thickness compression strength was 115.5±2.3 MPa.

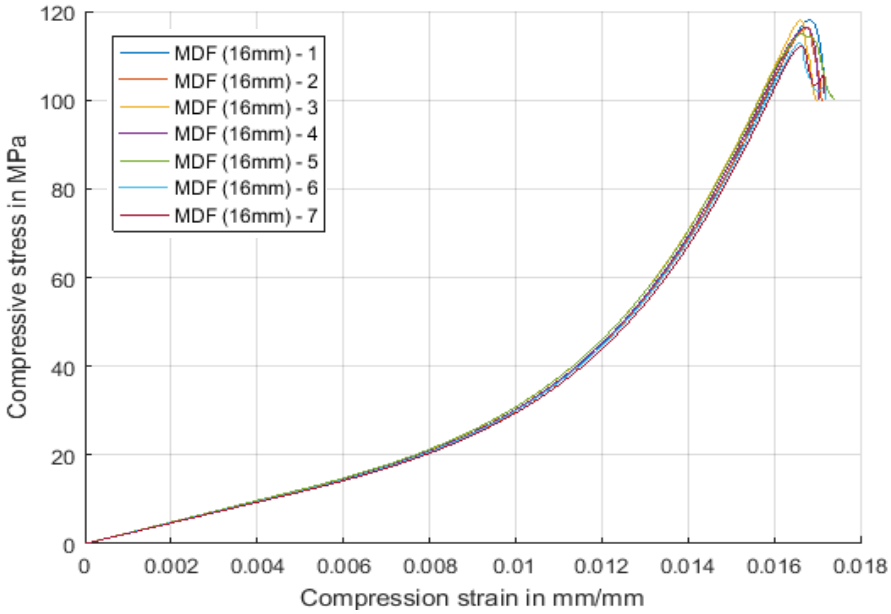

Figure 6: Engineering stress-strain curves obtained from through-thickness compression tests on 16 mm thick MDF blocks

In summary, the quasi-static material tests on MDF shows that the board had very consistent properties in flexure and through-thickness compression. The in-plane tensile properties were dominated by the more densified outer regions of the cross-section, with a relatively small influence from the orientation of the specimen relative to the MDF board. The flexure, through thickness and in-plane tension results gave confidence that the properties of the blast test specimens will be consistent during the explosive detonation experiments. However, the in-plane tension tests also revealed that the cross-section properties were not homogenous with respect to density, tensile strength and stiffness, creating challenges for detailed numerical modelling. Through-thickness tensile properties were lower and more variable than expected.

3. Blast test design

3.1 Blast test method

Small scale blast experiments involved detonating cylindrical disk-shaped charges of PE4 plastic explosive at the open end of a 200 mm long square section blast tube, as shown in Figure 7. The blast tube was employed to increase the spatial uniformity and decrease the intensity of the blast wave, similar to the method used in Langdon et al [30]. It also ensured that all the blast impulse was applied directly to the panels and not to the clamps. The cylindrical disks were placed on a polystyrene pad that fitted into a recess at the open end of the tube, allowing for precise location of the charge. The disks were detonated from the rear in the radial centre using an electrical detonator. A 300 mm by 300 mm MDF panel was mounted to the rear of the blast tube using picture frame clamps with six equi-spaced holes along each edge, for facilitating mountings and positioning. Prior to drilling the holes, each panel weighed 1.13 kg and had a mean thickness of 16.1 mm. The exposed area of the panel was 200 mm by 200mm, determined by the internal dimensions of the square tube. The front clamp frame was integral with the tube and the rear clamp frame was mounted onto pendulum via and adapter plate.

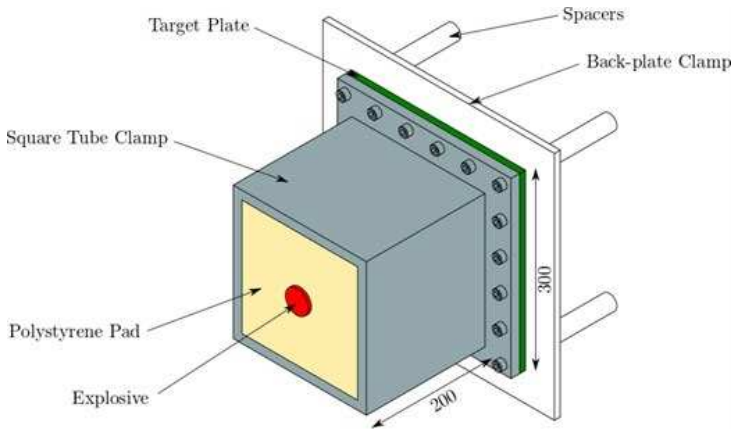

(a)

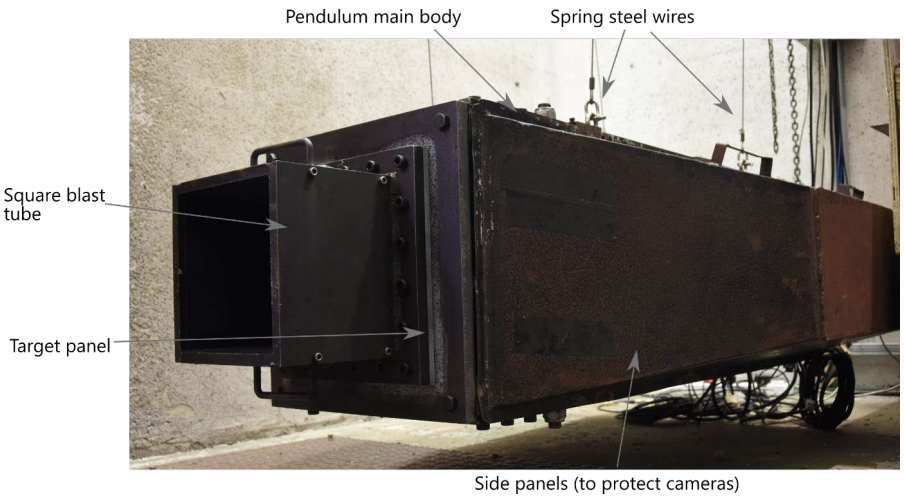

(b)

Figure 7: Blast loading experimental arrangement (a) schematic showing the charge positioning (b) photograph of the pendulum used to mount the specimen and determine impulse

3.2 Determining the explosive charge mass range

Basic computational simulations of the experiments were performed to determine a suitable charge mass range and disk diameter for the blast experiments. LS Dyna [31], a commercially available solver, was used to perform ¼ symmetry simulations of the experiments using the geometry described in Section 4.1. The multi-material arbitrary Lagrangian-Eulerian (MMALE) approach was adopted.

3.2.1 Geometry

To reduce run-times, only the exposed area of the panel was modelled while the clamped boundary was approximated by fully fixing the nodes along the appropriate edges, as shown in Figure 8. This was considered acceptable as the MDF panels exhibited little ductility in the material tests and the model was used for test design rather than detailed analysis. The walls of the blast tube were replaced with reflective boundaries. The explosive charge was situated 200 mm away from the MDF panel with a 50 mm region of air around and behind the explosive. Flow-out boundaries were used for the air outside the blast tube domain. A 50 mm region of air was modelled behind the MDF panel, also with flow-out boundaries. The air block meshes had solid elements with a side length of 2 mm, consistent with other blast modelling work [32-33]. The 16 mm thick MDF panel was modelled using solid elements, 1 mm by 1 mm by 1 mm, to prevent leakage while maintaining numerical accuracy, based on the recommendations in [31] and the mesh sensitivity study by [34].

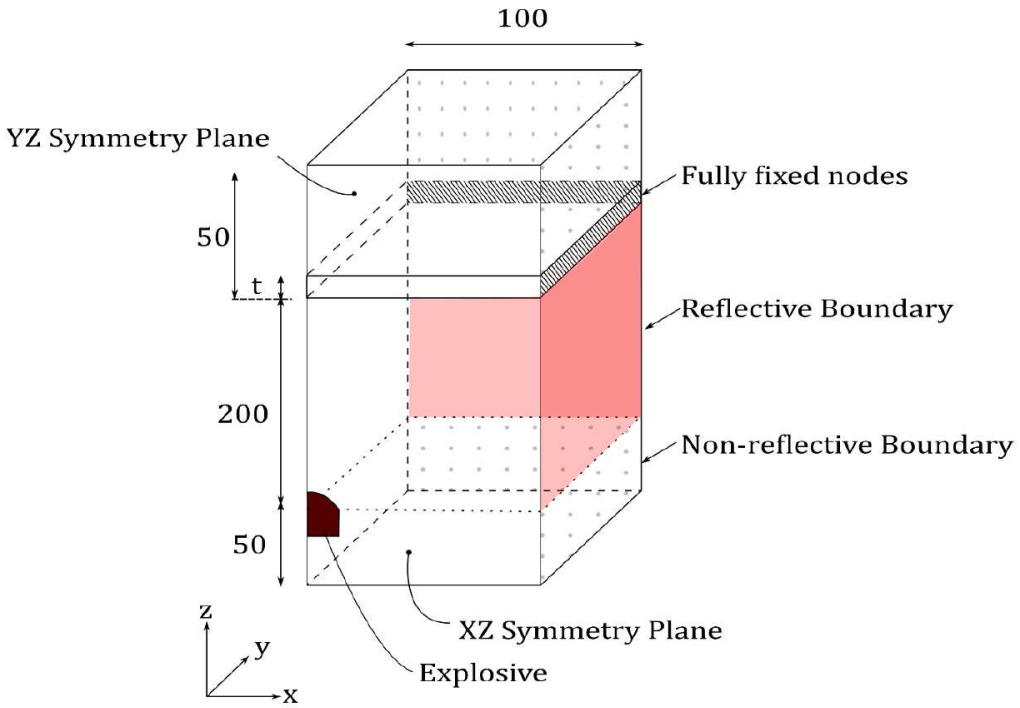

Figure 8: Schematic of basic geometry of MDF panel subjected to an explosive detonation (where t = panel thickness; for GLARE t = 1.41 mm, for MDF t = 16 mm)

3.2.2 Material modelling

Air was modelled as an ideal gas with an initial air density of 1.184 kg/m^3, a specific heat ratio of 1.4 and initial internal energy per unit volume of 253.3 kJ/m^3 [32, 35]. The explosive disk was modelled using the JWL equation of state, given by Eq (1). Following references [32-33, 35-37], the JWL parameters for C4 were used [33]. C4 and PE4 contain similar proportions of the active explosive RDX (C4 contains 91%, PE4 has 88%). Bogosian et al [38] determined that, for impulse and pressure equivalence, the two explosives can be treated as the same material. Details of the C4 JWL parameters are in Table 2.

$$p = a\left(1 - \frac{\omega}{R_1 V}\right)e^{-R_1 V} + B\left(1 - \frac{\omega}{R_2 V}\right)e^{-R_2 V} + \frac{\omega E}{V} \quad (1)$$

Table 2: Properties of C4 used in the simulations

Density (kg/m^3)	**a (GPa)**	**B (GPa)**	**R_1**
1601	609.77	12.95	4.5
R_2	**ω**	**D (m/s)**	**P_{CJ} (GPa)**
1.4	0.25	8193	28

The material characterisation experiments showed that the properties of the MDF cross-section varied between the relatively stiff and stronger denser outer regions with a relatively flexible core. Unfortunately, the transition in density between the inner and outer region is gradual, so the cross-section was modelled as a homogenous material with smeared properties. An isotropic elastic failure model (MAT13 in LS Dyna) that deleted elements when the strain exceeded a pre-defined value (0.5%, from Section 2.4) was used as a guide to indicate when the panels would be likely to fail in ways that would place the imagining system at risk. The estimated material properties are shown in Table 3. The shear modulus (G) and bulk modulus (K) were calculated using a Young's modulus (E) of 4 GPa and a Poisson's ratio (υ) of 0.25 [8].

Table 3: Smeared properties for MDF in MAT13 model

Nominal density (kg/m^3)	**Shear modulus (GPa)**	**SIGY[1] (MPa)**	**Bulk modulus (GPa)**
780	1.6	18	2.67

[1] Since MDF has very limited ductility, the ultimate tensile strength from [37] was used.

3.2.3 Results

Simulations were run for a 30 mm diameter, 10g PE4 disk detonation. An initial model was constructed using a 1.4 mm thick GLARE panel from Langdon et al [30] to validate the blast loading part of the model against the global impulse transfer measured in their experiments. The advantage of using reference [30] was that the geometry of the panel (except the thickness) and the blast tube were identical to the proposed MDF experiments. The simulation predicted an impulse of 22.3 Ns, compared to the 25.5 Ns measurement, a variation of 12.5%. Given the preliminary nature of the model, this was considered acceptable. Next, the same detonation was simulated but using a nominally 16 mm thick MDF panel. The run was terminated after 550 μs, which was sufficient time for the blast load and structural response to develop.

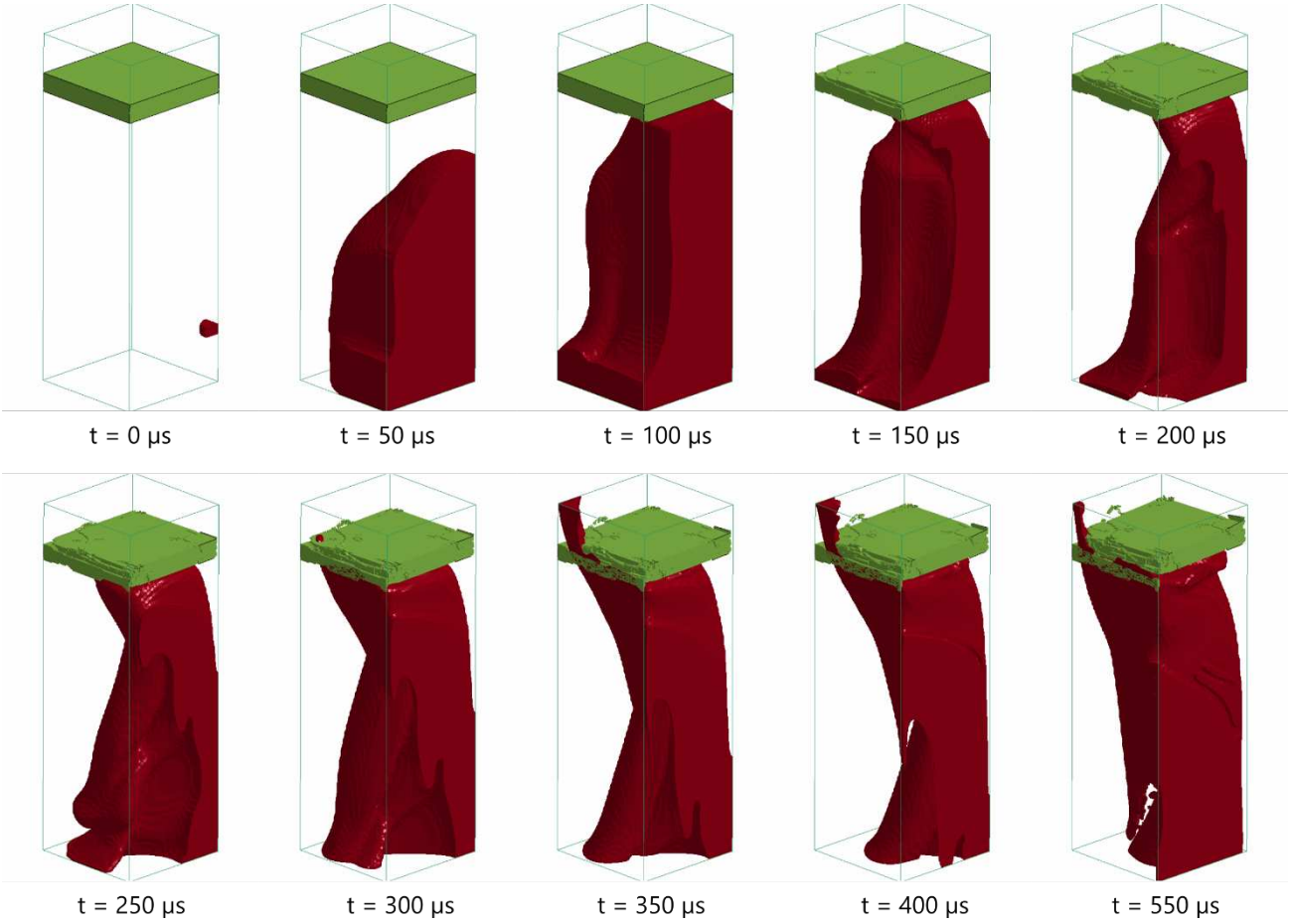

Figure 9: Simulation results showing blast development and panel damage (16 mm thick MDF panel, 10g charge detonation)

The development of the explosion and the panel damage, at selected time intervals, are shown in Figure 9. The detonation and blast wave development within the blast tube occurred during the first 50 μs (prior to impinging upon the panel). By 150 μs, many elements were deleted as the strain exceeded 0.5%, indicating that cracking within the panel would occur in reality. For the remainder of the simulation, increasing numbers of elements were deleted, denoting extensive cracking failure, with explosion products passing through a breech in the panel after 300 μs. The permanent displacement (18 mm, just over one plate thickness) predicted by the simulation

was somewhat meaningless due to the extensive damage. The simulations showed that a charge mass of 10g was too high, so the charge mass range was determined to be 2g to 6g PE4 based on the smallest quantity that could be reasonably detonated in the blast chamber using an electrical detonator.

3.3 Blast test measurements

The blast tube was mounted onto a horizontal pendulum with a single degree of freedom. The impulse was obtained by tracking the motion of the pendulum using a laser displacement sensor. Transient displacement across the mid-line of the panels was determined for two of the experiments using high-speed imaging equipment, shown in Figure 10. Two high-speed monochrome IDT NRS4 cameras, filming at 30 kfps, were mounted inside a modified pendulum and used to record the rear panel surface. Each camera was focused on the central strip through the middle of the test plate. Additional LED lights, covered by a diffuser, provided sufficient lighting to achieve good images for a 31 μs exposure time. The cameras were triggered using an aluminium foil break-wire circuit.

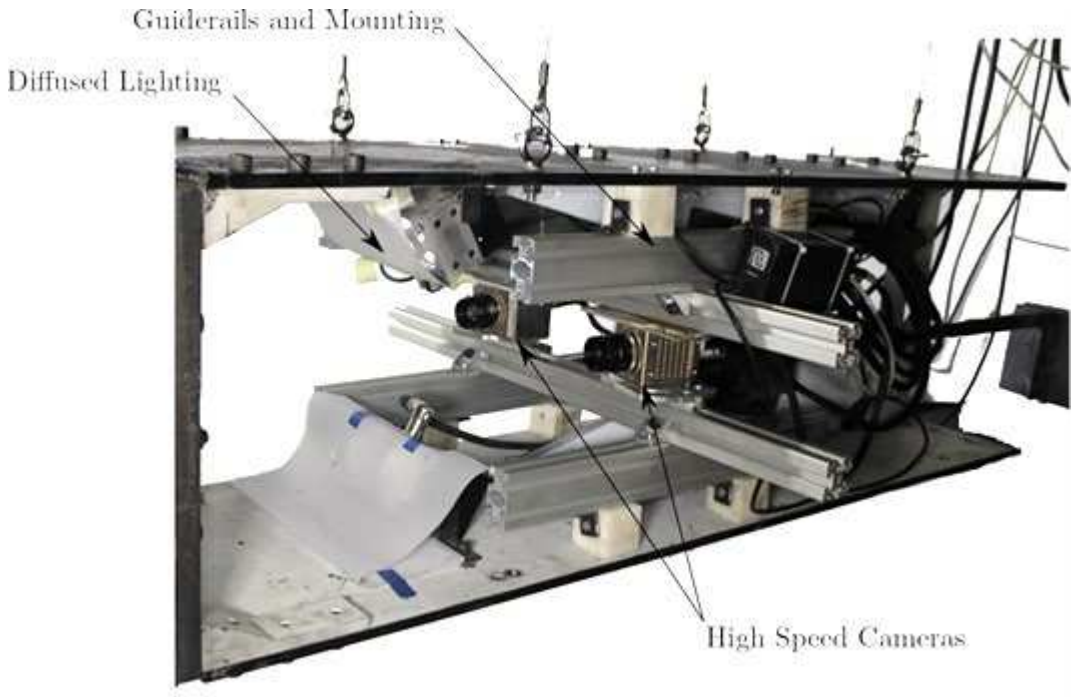

Figure 10: Photograph showing the high-speed camera system inside the modified pendulum

Prior to testing, the rear surface of the MDF panels was painted with a black and white speckle pattern, shown in Figure 11. The dotted yellow indicates the mid-line of the panel while the cross indicates the centre. Once the panel was mounted, the system was calibrated by recording approximately 8-10 images of a checkerboard calibration target at different positions (using both cameras) and processing the images in the DIC software using the pinhole model. The projection parameter of the entire system and additional distortion parameters were calculated. All analyses were performed using a subset size of 19 x 19 pixels and a grid spacing of 2 pixels,

similar to large deformation measurements captured using high speed stereovision system and DIC by others [40-42]. After testing, DIC was used to extract the displacement-time history of the mid-point and the evolution of the deformed mid-line profile at discrete times. Further details regarding the camera system and the DIC processing are available in Curry and Langdon [42]. After each test, the front and back surfaces of the target plates were visually inspected and photographed. Surface cracks were traced out and measured, then the panels were sectioned along the mid-line. Microscopy was used to elucidate the failure within the cross-section at higher magnifications when required.

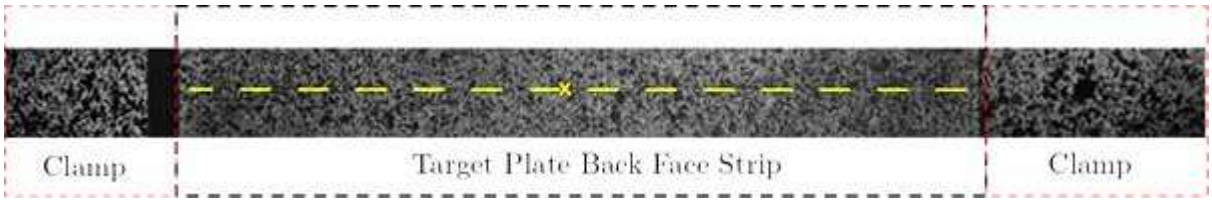

Figure 11: Photograph of a typical rear surface speckle pattern on the mid-line of the MDF panel (regions in red are within the clamp frame)

4. Results and discussion

Nine blast tests were performed at charge masses between 2g and 6g, including repeated tests at 3g, as shown in the results summary in Table 4. Two of the experiments using the high-speed imaging system to obtain transient responses. The charge diameter was reduced to 20 mm for most of the experiments; this was shown not to influence the impulse generated (identical impulses were generated by tests with 3.5g PE4 for the two diameters), but it allowed for smaller explosive charge detonations. There was an increase in impulse with increasing charge mass, as expected.

Table 4: Summary of blast test results

Specimen Name	Thickness (mm)	Charge mass (g)	Charge diameter (mm)	Impulse (Ns)
MDF-3.1	16.2	2	20	10.4
MDF-3.2	16.2	3	20	14.1
MDF-6	16.2	3	20	11.5
MDF-7	16.1	3	20	11.8
MDF-2	16.1	3.5	30	17.2
MDF-4	16.1	3.5	20	17.2
MDF-8	16.2	4	20	15.7
MDF-5	16.1	4.5	20	19.5
MDF-1	16.1	6	30	20

4.1 Transient response

The transient behaviours of two panels, from a test at 3g (MDF-7) and 4g (MDF-8) were successfully captured using the camera system and DIC analysis. For charge masses above 4g, extensive cracking in the panel meant the camera system was unable to record useful information. The mid-point displacement-time histories for the 3g and 4g tests are shown in Figure 12. At 3g (11.8 Ns impulse) the displacement peaked at 6.6 mm after 1.0 msec, and then rebounded to a minimum displacement of -4.3mm (that is, in the direction towards the detonation position), due to the elasticity of the material. The peak displacement was 4-5 times the permanent displacement measured post-test (approximately 1.5 mm). Several post-peak displacement oscillations were captured between 2 msec and 10 msec, from which a peak-to-peak damped period of oscillation was found to be approximately 2.9 msec. The deformed panel profiles for a 3g test is shown in Figure 13a. The transient mid-line profile is dome-shaped for all time intervals, with only the magnitude and direction varying through the oscillatory response.

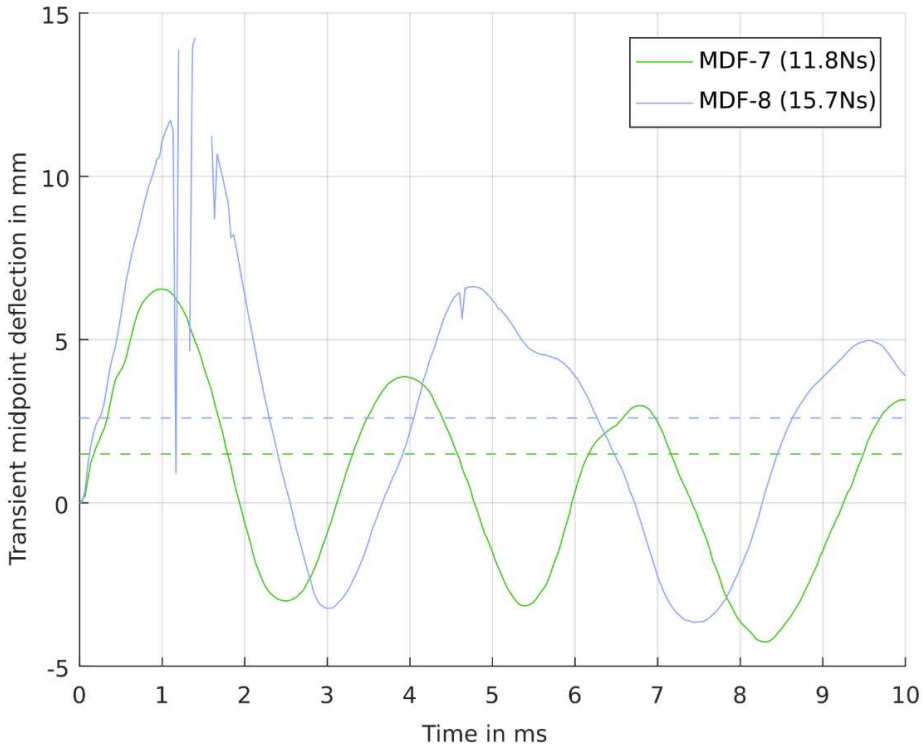

Figure 12: Graph showing experimentally determine transient mid-point displacement-time histories

For the 4g test (MDF-8, 15.7 Nm impulse), the peak displacement exceeds 11 mm after 1.1 msec but there is a break in the displacement-time history until a time of 1.7 msec. Stills taken from the camera footage show that a crack had developed on the rear surface of the panel after 1.1 msec, shown in Figure 14. The transient mid-line profiles, shown in Figure 13b, show a dome-shaped profile in the early part of the response (labelled 1) that becomes more conical-shaped after cracking, indicated by the straightened sides of the deformed profile (curves labelled 2 and 3). The crack creates a discontinuity in displacement in the panel centre. Hence, the "break" shown in Figure 12 is due to the crack that caused a discontinuity in the speckle pattern (meaning that

an accurate peak displacement could not be measured). Upon rebound, the crack appeared to close and DIC software was able to track the speckle pattern movement thereafter, the crack is still present in the subsequent deformed profiles (the slight ripple in Figure 13 at a time of 1.42 msec, for example). The post-peak displacement oscillated with a longer peak-to-peak duration of approximately 4.2 msec, indicating that the cracking and/or internal damage caused a loss of stiffness in the MDF. The peak displacement (above 11 mm) is more than four times the maximum permanent displacement (approximately 2.5 mm).

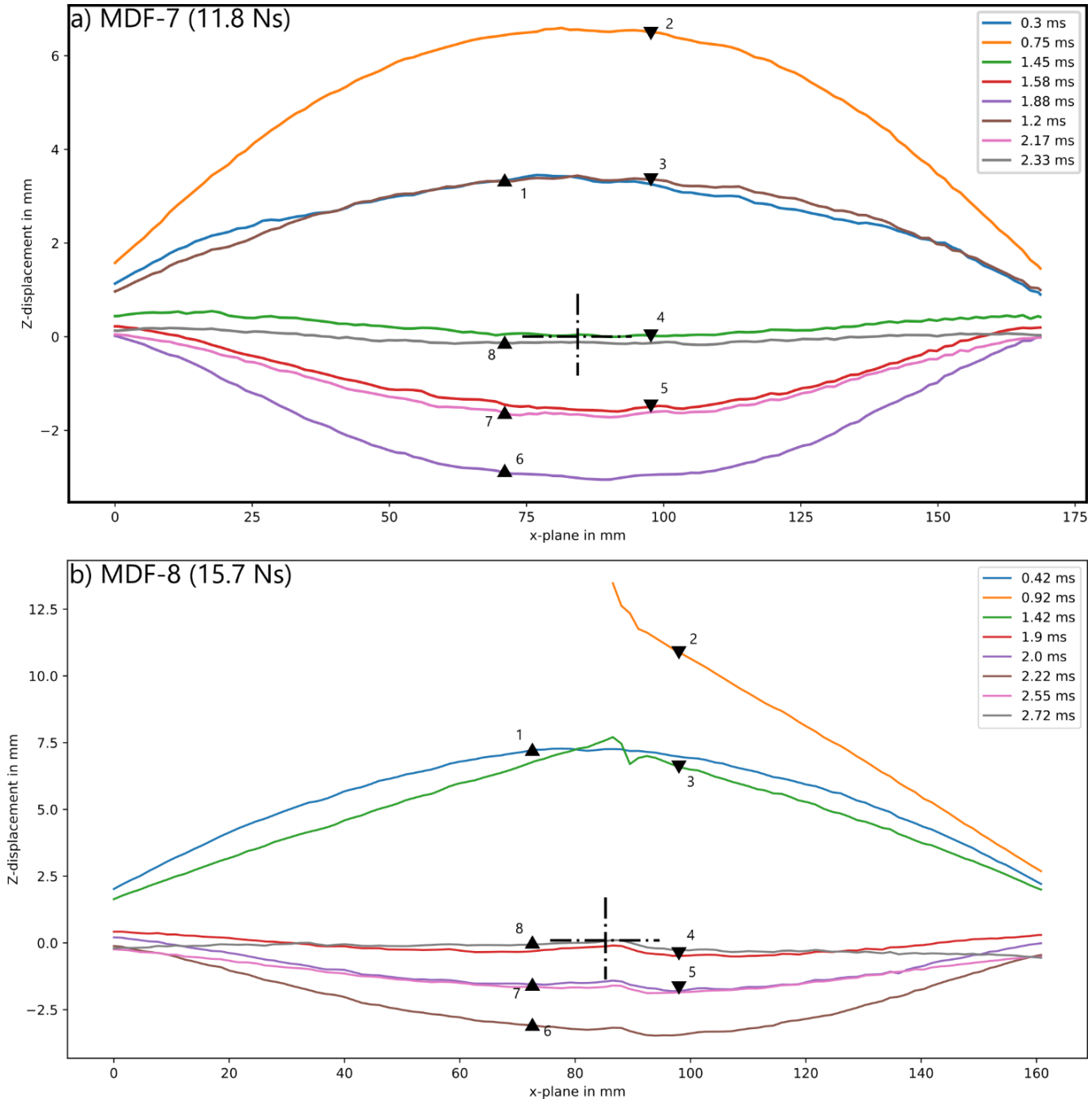

Figure 13: Deformed panel profiles at discrete times during the response obtained from DIC analysis, where the cross indicates the panel centre and the triangles indicate the direction of motion (a) test MDF-7, 3g (b) test MDF-8, 4g showing effect of cracking on transient plate profile

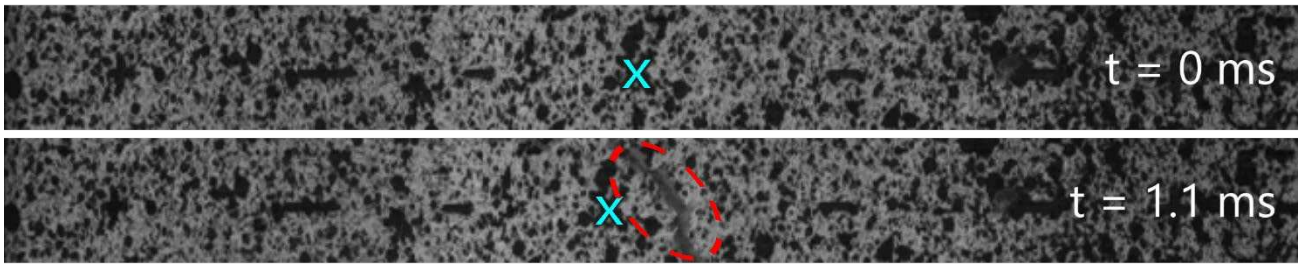

Figure 14: Stills taken from camera footage, showing crack development after 1 msec in MDF-8 (4g)

4.2 Surface damage

Views of the front and back surfaces of selected blast-tested panels are shown in Figure 15, with images ordered by increasing impulse (charge mass range 3-6g) from left to right. The front surfaces are discoloured by the residue from the blast products (the blackened areas) and not from charring of the MDF.

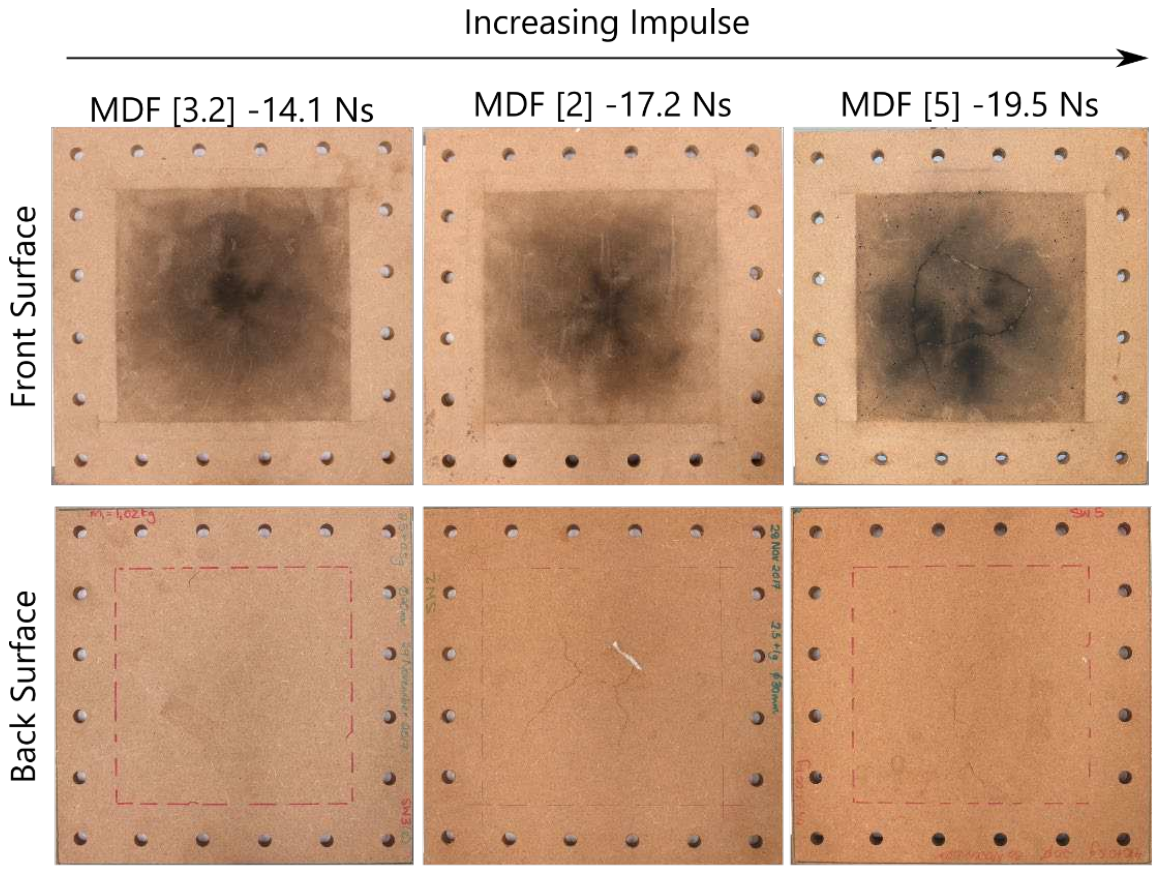

Figure 15: Photographs of the front and back surfaces of selected panels

Cracks on the panel surfaces were measured during post-test inspection, and traced in red on digitised images, as shown in Figure 16. Multiple cracks on the rear surface of all the panels are visible, clustered around the central region of the exposed area. Similar cracking is present on the front surface of MDF-5 (4.5g, 19.5 Ns); for this test, the cracking extended to the boundary on both sides and appeared circular in the central region of the front surface. The length of the cracks increased with charge mass (although not precisely a linear trend) but there was no particular trend in the cracking pattern.

Test panel MDF-1 was completely breeched at 20 Ns (6g), shown in Figure 17, with cracking, delamination and fragmentation evident throughout the panel. The mass lost was approximately 180 g (more than 1/3 of the mass of the panel region exposed to the loading) for panel MDF-1 due to this fragmentation. These results have implications for blast protection. Although MDF is a commonly used construction material, it offered little protection in the event of an explosive detonation. However, the MDF fragmentation process could lead to secondary blast injuries [43]. In other words, during explosion events, flying debris causes blunt force and penetrating trauma [44]. Fragments from MDF furniture in buildings in "real-life" explosions could result in additional injuries to people nearby.

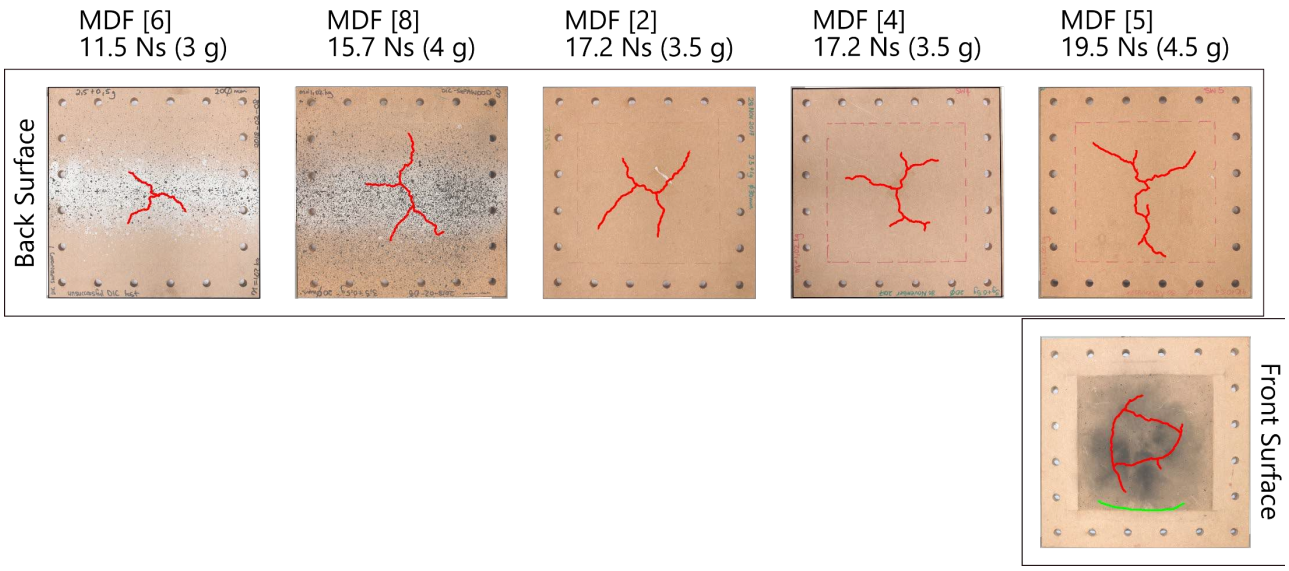

Figure 16: Cracking patterns on the front and rear surfaces of the blast-tested panels (shown in red)

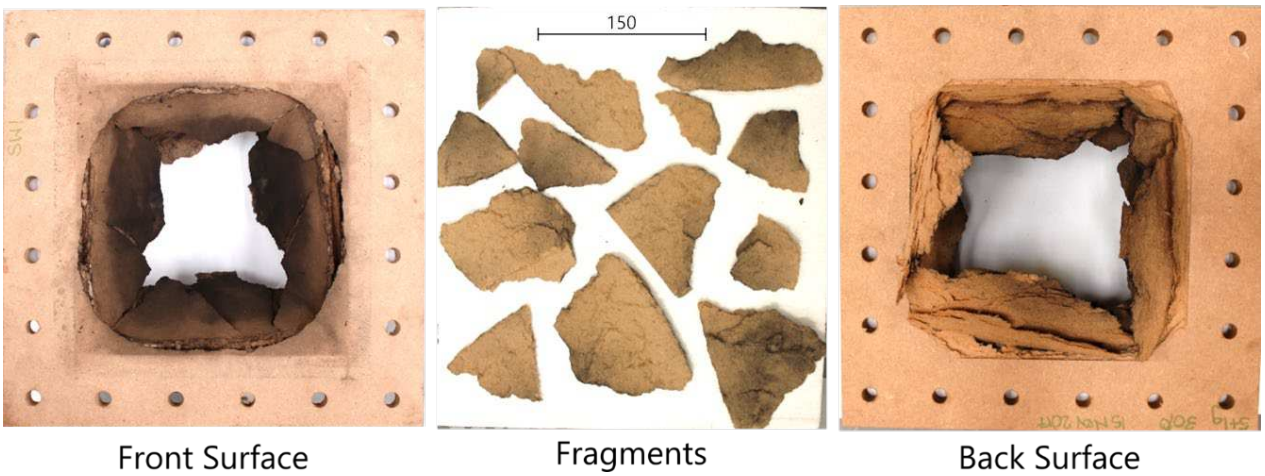

Figure 17: Photographs showing the fragmentation of panel MDF-1 (6g, 20 Ns)

4.3 Cross-section damage

In-plane cracking failures were observed within the cross-sections of all the tested panels, running along the entire mid-line. The cracks in panels tested at the lowest charge mass were found in the less densified core. It appeared that in-plane cracks initiate in weaker (lower density) regions of the cross-section, as might be expected. As the charge mass increased, the number of in-plane cracks increased until the outer few millimetres of the rear surface began to delaminate from the rest of the panel (for example, MDF-5, 4.5g, in Figure 18). Microscope images shown in Figure 19 show magnified views of the cracking. The in-plane cracking separates layers of fibres, seen in Figure 19a. A top view of the crack, Figure 19b, shows a clean break, with very few fibres disturbed by the layer separation.

Figure 18: Photographs of panel cross-sections (in order of increasing charge mass, from bottom to top, with panels arranged so that the front surfaces were on the bottom)

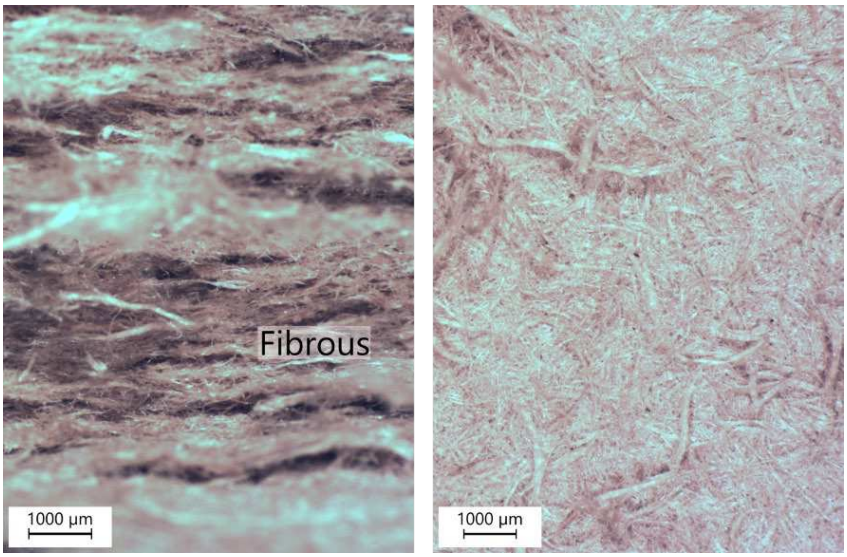

(a) (b)

Figure 19: Microscope images of fracture surfaces (a) cracking through the panel thickness (b) top surface view of a crack

Concluding comments

The transient and response of MDF panels subjected to air-blast loading was investigated through a series of small-scale, carefully controlled explosive detonation experiments. MDF exhibited extremely poor blast resistance and very brittle response, consistent with its relatively low quasi-static strength and ductility. Panels exhibited multiple surface cracks and in-plane cross-section cracks at low explosive charge masses. Transient response measurements showed the panels has peak displacements of up to five times their final displacement, and that cracking damage within the panel caused a reduction in its stiffness (evidence from examining the post-peak elastic oscillation period). Crack initiation also affected the deformed shaped of the panel; as a crack opened, the deformed profile changed from a dome-shape to something more conical and then reverted to a dome upon elastic rebound. At higher charge masses, cracking became more extensive. A panel breech occurred at 6g, with more than a third of the exposed mass of the panel fragmenting during the breech.

These findings should prove useful to those modelling structural response following a blast event, with cracking and fragmentation failures being the main failure types that must be included in the material formulation. MDF fragmentation should not be disregarded by those modelling damage and injury risks due to the increased secondary injury risk from flying debris.

Acknowledgements

The authors are grateful to the National Research Foundation (NRF) of South Africa for their financial support. Opinions expressed and conclusions arrived at, are those of the authors and are not necessarily to be attributed to the NRF. The authors would also like to thank the staff of the Mechanical Engineering workshop at UCT for their assistance in machining the specimens and pendulum parts.

Data availability statement

The raw and processed data required to reproduce these findings cannot be shared at this time due to technical or time limitations.

References

1. Institute for Economics & Peace. Global Terrorism Index 2020: Measuring the Impact of Terrorism, Sydney, November 2020. Available from: http://visionofhumanity.org/reports (accessed 5/2/2021).
2. BBC, *Sri Lanka attacks: what we know about the Easter bombings*, April 2019. https://www.bbc.co.uk/news/world-asia-48010697
3. I. Overton, J. Dathan, C. Winter, J. Whittaker, R. Davies, M. Q. Kaaman, H. Kaaman, Improvised explosive device monitor 2017, *Action on Armed Violence, Tech. Rep.,* 2017.
4. BBC, *China industrial park explosion kills 19*, July 2018. https://www.bbc.com/news/world-asia-china-44816715
5. N. Osseiran, I. Coles. Beirut Explosion: What Happened in Lebanon and Everything Else We Know, *Wall Street Journal*, 2020. Available from: https://www.wsj.com/articles/beirut-explosion-what-happened-in-lebanon-and-everything-else-you-need-to-know-11596590426
6. S.E. Rigby, T.J. Lodge, S. Alotaibi, A.D. Barr, S.D. Clarke, G.S. Langdon, A. Tyas. Preliminary yield estimation of the 2020 Beirut explosion using video footage from social media. *Shock Waves* 30:671–675, 2020.
7. E.M. Fernandes, V.M. Correlo, J.A.M. Chagas, J.F. Mano, R.L. Reis, Properties of new cork–polymer composites: Advantages and drawbacks as compared with commercially available fibreboard materials, *Compos Struct*, 3(12):3120-3129, 2011.
8. Forest Products Laboratory. *Wood Handbook: Wood as an Engineering Material,* General Technical Report FPL-GTR-190, USDA Forest Service, 2010.
9. C.M. Pekarski, A.C de Francisco, L.M. da Luz, J.L. Kovaleski, D.A.L. Silva. Life cycle assessment of medium-density fibreboard (MDF) manufacturing process in Brazil, *Sci Total Envir*, 575:103-111, 2017.
10. Healthy Building Network, Alternative Resin Binders for Particleboard, Medium Density Fiberboard (MDF) and Wheatboard, 2008. Available: https://news.bio-based.eu/media/news-images/20090216-02/Alternative_Resin_Binders.pdf
11. X. Li, Y. Li, Z. Zhong, D. Wang, J.A. Ratto, K. Sheng, X.S. Sun, Mechanical and water soaking properties of medium density fiberboard with wood fiber and soybean protein adhesive, *Bioresource Techn*, 100(14):3556-3562, 2009.
12. S. Halvarsson, H. Edlund, M. Norgren, Properties of medium-density fibreboard (MDF) based on wheat straw and melamine modified urea formaldehyde (UMF) resin, *Industrial Crops & Products* 28(1):37-46, 2008.

13. Firm claims breakthrough in recycling of MDF waste, *Envirotec Magazine*, 2017. Available: https://envirotecmagazine.com/2017/01/16/firm-claims-breakthrough-in-recycling-of-mdf-waste/ (accessed 6/2/2021)
14. A. Ghazlan, T. Ngo, P. Tran, V.T. Le, T. Nguyen, A.S. Whittaker, A. Remennikov. Enhancing Toughness of Medium-Density Fiberboard by Mimicking Nacreous Structures through Advanced Manufacturing Techniques. *J Struct Engng*, 146(3): 04020001, 2020.
15. W. Gul, A. Khan, A. Shakoor, Impact of Hot Pressing Temperature on Medium Density Fiberboard (MDF) Performance, *Adv in Mater Sci Engng*, 4056360, 2017.
16. N. Ayrilmis, S. Jarusombuti, V. Fueangvivat, P. Bauchongkol. Effects of thermal treatment of rubberwood fibres on physical and mechanical properties of medium density fibreboard, *J. Tropical Forest Sci* 23(1):10-16, 2011.
17. E. Mahrdt, H.W.G. van Herwijnen, W. Kantner, J.Moser, J. Giesswein, R. Mitter, U. Müller, W.Gindl-Altmutter, Adhesive distribution related to mechanical performance of high density wood fibre board, *Int J Adhesion & Adhesives*, 78:23-27, 2017.
18. D. Lacroix, C. Viau, D. Côté, M. Poulin, A. Lopez, G. Doudak, Overview on the structural performance of timber structures under the effects of blast loading & research and design considerations, *Struct & Architecture*. CRC Press, 67–74, 2016.
19. J. Buchar, L. Severa, M. Havlicek, S. Rolc. Response of wood to the explosive loading, *J. Phys. IV JP*, 10(9): 529–534, 2000.
20. A.P. Bol'shakov, , M.A. Balakshina, N.N. Gerdyukov, E.V. Zotov, A.K. Muzyrya, A.F. Plotnikov, S.A. Novikov, V.A. Sinitsyn, D.I. Shestakov, Y.I. Shcherbak. Damping properties of sequoia, birch, pine, and aspen under shock loading. *J. Appl. Mech. Tech. Phys.*, 42(2): 202–210, 2001.
21. N.J. Parlin, W.G. Davids, E. Nagy, T. Cummins, Dynamic response of lightweight wood-based flexible wall panels to blast and impulse loading, *Construct & Building Mater*, 50:237-245, 2014.
22. V.T. Le, A. Ghazlan, T. Nguyen, T. Ngo. Performance of bio-inspired cross-laminated timber under blast loading - A numerical study, *Compos Struct* 260:113524, 2021.
23. PG Bison, Supawood, 2020. Available: https://pgbison.co.za/products/supawood (accessed 6/2/2021).
24. PG Bison, Supawood MDF Material Safety Data Sheet, 2017. Available: https://pgbison.co.za/sites/default/files/2020-03/SupaWood%20Material%20Safety%20Data%20Sheet.pdf (accessed 6/2/2021).
25. ASTM International, *D7264/D7264M-15 Standard Test Method for Flexural Properties of Polymer Matrix Composite Materials*, West Conshohocken, PA, 2015.
26. ASTM International, *D3039/D3039M-17 Standard test method for Tensile Properties of Polymer Matrix Composite Materials*, West Conshohocken, PA, 2014.
27. South African National Standard, *SAN 6016:2005 Transverse tensile (internal bond) strength of wood-based panels*, Groenkloof, 2011.
28. South African National Standard, *SANS 540-1:2009 Fibreboard products Part 1 : Uncoated fibreboard*, Groenkloof, 2009.

29. ASTM International, *D1037-12 Standard test methods for evaluating Properties of Wood- Based Fiber and Particle Panel Materials*, West Conshohocken, PA, 2012.
30. G.S. Langdon, Y. Chi, G.N. Nurick, P. Haupt, Response of GLARE© panels to blast loading, *Eng Struct* 1(12):3116–3120, 2009.
31. Livermore Software Technology Corporation, *LS-DYNA Keyword User's Manual Volume II R7.1*, no. 5442. Livermore, California, 2014.
32. G.S. Langdon, A. Ozinsky, S. Chung Kim Yuen. The response of partially confined right circular stainless steel cylinders to internal air-blast loading, *Int J Impact Eng*, 73:1-14, 2014.
33. S.C.K. Yuen, A. Butler, H. Bornstein, A. Cholet, The influence of orientation of blast loading on quadrangular plates, *Thin-Walled Struct*, 131:827–837, 2018.
34. G. Volschenk, The response of aluminium and glass fibre FMLs subjected to blast loading, *MSc dissertation*, University of Cape Town, 2015.
35. B.M. Dobratz. *LLNL explosives handbook: properties of chemical explosives and explosives and explosive simulants* (No. UCRL-52997). Lawrence Livermore National Lab., USA, 1981.
36. L. Schwer, S.E. Rigby. Secondary and height of burst shock reflections: application of afterburning, *Proc. 25th Military Aspects of Blast and Shock*, 2018.
37. J. Lee, E.L. Hornig, H.C. Kury, Adiabatic expansion of high explosive, 1968. doi:10.2172/4783904.
38. D Bogosian, M Yokota, SE Rigby, TNT equivalence of C-4 and PE4: a review of traditional sources and recent data, *24th Military Aspects of Blast and Shock*, Nova Scotia, Canada, 2016
39. Medium density fibreboard, 2021. Available from: https://www.makeitfrom.com/material-properties/Medium-Density-Fiberboard-MDF
40. H. Schreier, J.-J. Orteu, M.A. Sutton, *Image Correlation for Shape, Motion and Deformation Measurements*. Boston, MA: Springer US, 2009.
41. M.A. Sutton, Three-dimensional digital image correlation to quantify deformation and crack-opening displacement in ductile aluminum under mixed-mode I/III loading, *Opt. Eng.*, 46(5): 051003, 2007.
42. R.J. Curry, G.S. Langdon, Transient response of steel plates subjected to close proximity explosive detonations in air, *Int J Impact Engng*, 102: 102-116, 2017.
43. US Department of Defense (DoD). *DoD Directive 6025.21E: Medical research for prevention, mitigation, and treatment of blast injuries*, 2006.
44. J.M. Wightman, S.L. Gladish. Explosions and blast injuries. *Ann Emerg Med*. 37(6):664-678, 2001.